EXPERIMENTAL STUDY OF ELM CONTROL BY VARYING TOROIDAL ROTATION WITH CTR-NBI ON EAST

D. KONG
Institutes of Plasma Physics, CAS,
People's Republic of China Hefei 230031
Email: dfkong@ipp.ac.cn

C. HUANG[2], X. GAO[1], B. LYU[1], L. WANG[1], T. ZHANG[1], Z. LIU[2], A. LIU[2], T. LAN[2], Y. DUAN[1], L. ZHANG[1], J. LI[1] and the EAST team
1) Institutes of Plasma Physics, CAS, Hefei 230031, People's Republic of China
2) University of Science and Technology of China, Hefei 230026, People's Republic of China

Abstract

A non-stationary, effective edge localized modes (ELMs) mitigation/suppression regime has been recently obtained by counter current direction NBI heating on the Experimental Advanced Superconducting Tokamak (EAST). By scanning toroidal rotation with a combination of co-current direction NBI, counter-current direction NBI and radio-frequency heating, it is found the ELM-induced particle and ELM frequency decrease with increasing toroidal rotation in counter current direction. The synergistic effect of rotation and collisionality on ELM behavior was studied by statistical analysis, which is consistent with previous nonlinear BOUT++ simulation result. A ballooning-like mode which replaced ELMs is found in the pedestal region in ELM mitigation/suppression regime, yet it is inefficient in producing particle and energy transport to maintain a stationary confinement. These results suggest a possible way to reduce energy and particle losses by ELMs and maintain quasi-stationary state by modulation of co-current direction NBI and counter-current direction NBI.

1. INTRODUCTION

High confinement mode (H-mode) is characterized by formation of edge transport barrier in a narrow edge region inside the separatrix called pedestal, and subsequent confinement improvement over low confinement mode (L-mode). The edge-localized modes (ELMs), a ubiquitous feature of H-mode, induce periodic and impulsive particle transport outwards. Owing to its high confinement as well as broad experimental and theoretical basis, ELMy H-mode regime is selected for ITER Q~10 scenario ($Q=P_{fus}/P_{in}$, the amplification factor)[1]. ELMs are beneficial for steady-state operation in a way of providing density control, preventing impurity accumulation and sustaining plasma performance. On the other hand, the intensive heat pulses induced by high power (type-I) ELMs may erode plasma facing components and degrade performance. It is estimated that unmitigated type-I ELMs in ITER 15 MA Q~10 scenario could correspond to a maximum ELM heat flux of 0.5 MJm^{-2}, which would cause significant cracking of the tungsten (W) surface[2].

In recent years, a concerted worldwide effort has emerged to develop efficient and reliable ELM control techniques. These techniques include ELM mitigation by ELM pacing using pellet injection (PI) [3] or vertical kicks [4], and ELM suppression by applying resonant magnetic field perturbations (RMP) near the plasma edge [5]. Another possibility would be operation in a naturally small or no ELMs regime such as quiescent H-mode (QH-mode) [6]. QH-mode is high performance ELM-stable H-mode, generally accompanied by a coherent edge harmonic oscillation (EHO) which provides a continuous transport channel that maintains the pedestal just below the ELM stability boundary [6]. Theory indicates the EHO is a saturated kink/peeling mode driven by current density and edge rotational shear [7].

Experiments suggest that toroidal rotation or rotation shear in the edge can affect ELM behavior. Sufficient edge rotation shear by strong neutral beam injection (NBI) [8] or non-axisymmetric, non-resonant magnetic fields (NRMFs) [9] to provide necessary toroidal torque has been required to obtain QH-mode in DIII-D. In JT-60U, various combination of NBI lines was used to vary toroidal torque without changing absorbed power [10]. It was reported that the energy loss of type I ELMs and grassy ELMs was reduced and the ELM frequency increased with more counter-I_p torque, meanwhile the ELMy H-mode maintained good density control [11,12]. In this paper, we report the recent study of ELM control by using NBI in the direction counter to the plasma current in EAST. Section 2 presents the main experiment results and section 3 discusses possible explanations of ELM mitigation/suppression in terms of linear stabilization by toroidal shear and nonlinear coupling by large E_r.

2. CTR-NBI HEATING ELM CONTROL EXPERIMENT IN EAST

The Experimental Advanced Superconducting Tokamak (EAST) is medium size (major radius R=1.75 m and minor radius a=0.45 m) fully superconducting tokamak which aims at steady-state operation. EAST has two beam units (each consist of two ion sources) for positive ion based NBI with a maximum power of 8 MW (4×2 MW). A co-tangential unit at A Port named "co-NBI" and the other counter-tangential unit at F Port (named "ctr-NBI") can, respectively, inject toroidal momentum in the same direction as the plasma current and in the opposite direction to the plasma current. Lower hybrid wave (LHW) heating and ion cyclotron resonance heating (ICRH) are the principal RF heating and current drive schemes on EAST, which can deliver a maximum power of 10 MW and 12 MW, respectively.

A series of experiments has been carried out on EAST to study the impact of toroidal rotation on ELMs. The range of plasma current for all shots discussed in this paper is 0.4~0.5 MA and the range of toroidal magnetic field strength is 1.7~2.3 T, which corresponds to a range in q_{95} of 3.9~7.7. The direction of plasma current and toroidal magnetic field is counter-clockwise and clockwise, respectively, thus $B \times \nabla B$ points towards the lower divertor. The plasma configuration is in a standard lower single null (LSN) shape for EAST with elongation $1.6<\kappa<1.87$. Lithium wall coating has been applied before the experiment everyday [13].

The core plasma temperature and toroidal rotation velocity are obtained by measuring Ar XVII spectra using a tangential viewing image X-ray crystal spectrometer (TXCS) [14]. Due to unavailable accurate absolute wavelength calibration, rotation measurement is presented in the form of relative increment over L-mode phase, *i.e.* the rotation magnitude was subtracted by the average value in L-mode phase, which is assumed to be nearly zero. The impurity content is obtained by measuring impurity line emissions using a fast-time-response extreme ultraviolet spectrometer (XUV) [15]. The ELM-induced particle flux was measured by triple Langmuir probes array embedded in the divertor target plates [16]. The central line-averaged density and density profile are measured by hydrogen cyanide (HCN) far-infra laser interferometer and density profile Reflectometer [17], respectively. The edge radial electric field is measured by Doppler Reflectometer [18]. Figure 1 shows the position of NBI system and key diagnostics in this paper.

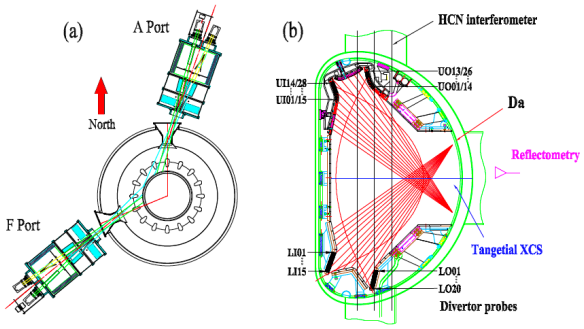

FIG 1. (a) Bird-view of EAST tokamak showing co-current direction NBI system at Port A and ctr-current direction NBI system at Port F. (b) Poloidal section of EAST tokamak showing position of key diagnostics including HCN interferometer, Reflectometry, D_α filterscope system, Tangential X-ray Crystal Spectrometer and divertor probes.

Figure 2 shows waveforms of co-NBI and ctr-NBI modulation discharge. In shot 55251, co-NBI and ctr-NBI heating is modulated with frequency of 1 Hz and duty cycle of 50%. The absorbed co-NBI and ctr-NBI heating power is about 0.4 MW and 0.5 MW, while the central toroidal rotation velocity with co-NBI and ctr-NBI heating is 40 km/s and -10 km/s, respectively. Radio-frequency heating power of LHW and ICRH are kept constant during current at stage (from 2 s to 14 s). In this shot, plasma density was kept fixed by SMBI density feedback during NBI modulation, and the stored energy was near constant with suitable $P_{ctr\text{-}NBI}/P_{co\text{-}NBI}$. The D_α signal indicated that the ELMs were greatly mitigated in ctr-NBI phase as shown in figure 2 (d,e). Note that the magnitude of the D_α spikes vary with central toroidal rotation velocity VT0. In terms of particle balance, much more outward particles were brought by ELMs in co-NBI phase compared with ctr-NBI phase, thus SMBI was applied mainly in co-NBI phase to keep plasma density constant. The radiation power P_{rad} begin to rise in ctr-NBI phase because of impurity accumulation, which will be discussed in details later.

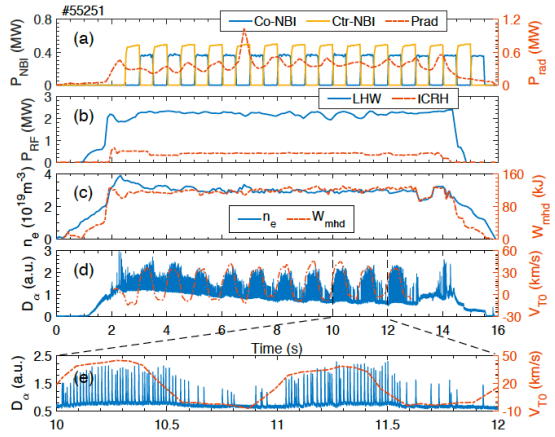

FIG 2. Waveform of co-NBI and ctr-NBI modulation shot (shot 55251): (a) co- and ctr-NBI heating power and radiation power P_{rad}, (b) radio-frequency wave heating power (LHW and ICRH), (c) line-averaged plasma density _ne and stored energy W_{mhd}, (d) D_α signal and central toroidal rotation velocity V_{T0}, (e) zoomed signal from (d).

In shot 54800, combination of four ion sources were utilized to ramp co-NBI and ctr-NBI heating power in steps, as shown in figure 3 (a). RF heating was applied to heat the bulk plasma. The normalized β_N in H-mode phase ranges from 1.0 to 1.5. By changing $P_{co\text{-}NBI}$ from 0.5 MW to 1.0 MW, the ELM frequency increased from 55 Hz to 100 Hz, in accordance with the frequency dependence of type-I ELMs with heating power. Remarkably, it is found both the ELM amplitude and frequency was reduced with increasing $P_{ctr\text{-}NBI}$ -$P_{co\text{-}NBI}$, i.e. the counter-Ip NBI torque, as shown in the zoomed D_α signal intervals in figure 3 (e-h). After turning off co-NBI, ELMs were suppressed with ctr-NBI and ELM-free H-mode became non-stationary with density climbing up.

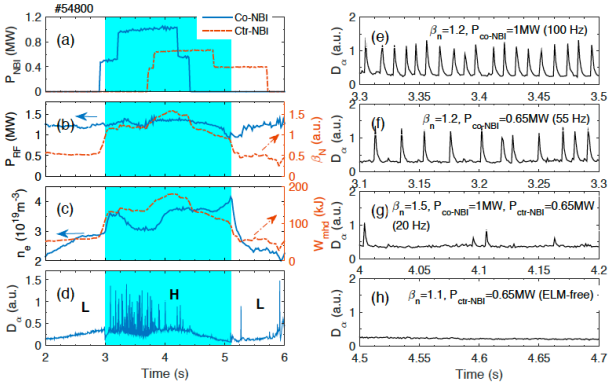

Figure 3. Waveform of NBI power ramp shot (shot 54800): (a) co- and ctr-NBI heating power, (b) radio-frequency heating power (LHW+ICRH) and β_N, (c) line-averaged plasma density $\bar{n}_e$ and stored energy W_{mhd}, (d) D_α signal, (e-h) zoom in $D_\alpha$signal in H-mode showing ELM mitigation and suppression with increasing $P_{ctr\text{-}NBI}-P_{co\text{-}NBI}$. The shaded area denotes H-mode phase.

In shot 56417 (figure 4), the co-NBI and ctr-NBI heating was applied separately. 1 MW LHW was applied to heat the bulk plasma during current at stage (from 2 s to 6 s), which was not plotted in figure 4. No density feedback by SMBI was applied in this shot. In contrast with stationary ELMy H-mode in co-NBI phase, the ELM-free H-mode in ctr-NBI phase has increased plasma density and degrade confinement (indicated by decrease of T_{e0}, T_{i0} and W_{mhd}). Impurity accumulation was observed (see figure 5), which resulted in increase of radiation power and finally H-L transition.

In figure 5, the radiation power normalized by density and impurity content in two typical shots are compared. In shot 55251 with NBI modulation, $P_{rad}/\overline{n_e}$Prad=_ne is increasing in ctr-NBI phase and decreasing in co-NBI phase, as well as the main impurity content like C, Mo and W. This demonstrates better impurity control by ELMs in co-NBI phase. In shot 56417 without NBI modulation, impurity content is kept low in co-NBI phase, and quickly increase in ctr-NBI phase. Comparison between with and without NBI modulation shows NBI modulation with appropriate duty time can be applied to reduce heat load in ELM-free H-mode with ctr-NBI, and expel impurity in ELMy H-mode with co-NBI. Notably, the abrupt increase of radiation power at t = 3.2s in figure 5 (e) is caused by dust (mainly Cu) dropped from upper divertor, which is not regularly seen in other shots.

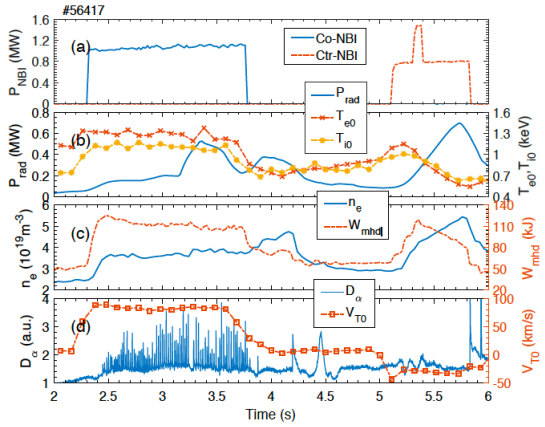

Figure 4. Waveform of co-NBI and ctr-NBI applied separately (shot 56417): (a) co-and ctr-NBI heating power (b) radiation power P_{rad}, core electron temperature T_{e0} and ion temperature Ti0, (c) line-averaged plasma density n_e and stored energy W_{mhd}, (d) D_α signal and central toroidal rotation velocity V_{T0}.

As direct measurement for edge toroidal rotation velocity is not available in EAST, the central toroidal rotation velocity is used instead. It is assumed the rotation velocity profile is stiff under different toroidal torque, i:e: edge toroidal rotation changes in the same way as central toroidal rotation does, as the case in JT-60U [10, 12]. Statistical analysis of the correlation between ELM characteristic (ELM size and frequency) and plasma parameters (V_{T0} and n_e) was done. The database contains 164 time intervals from 66 NBI-heating shots in campaign 2015. The time intervals last from 100 *ms* to 1000 *ms* according to the duration of applied NBI and the ELM characteristic do not change in each interval. Due to inaccurate data of heat flux, the ELM size is quantified by particle flux of ELMs $\Gamma_{ion,ELM}$. The calculating method is shown as follow [19, 20]. The particle flux is given by

$$\Gamma_{ion} = n_t C_{st} = \frac{j_s}{e} \tag{1}$$

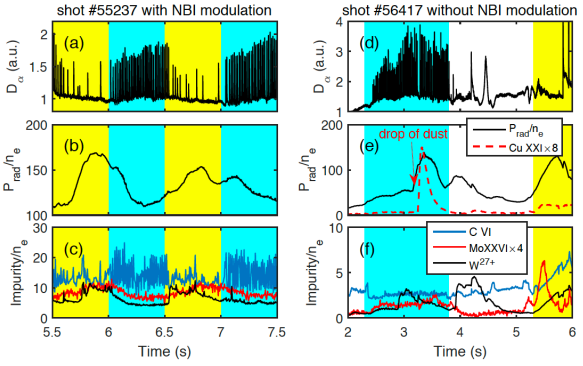

Figure 5. Waveform of (a) D_α signal, (b) radiation power divided by plasma density, (c) impurity intensity of C, Mo and Cu in shot 55237 with NBI modulation; and (d) D_α signal, (e) radiation power divided by plasma density (black line) and Cu impurity intensity (red dashed line), (f) impurity intensity of C, Mo and Cu in shot 56417 without NBI modulation. Radiation power is measured by fast bolometer and impurity intensity is measured by fast EUV spectrometer. The blue area and yellow area denotes co-NBI and ctr-NBI H-mode respectively.

where n_t, C_{st} and j_s are the electron density, ion sound speed and ion saturation current at the target, respectively. The total particle flux on the divertor targets is given by

$$\Gamma_{tot}(t) = \int_{s_a}^{s_b} 2\pi R_{div} \Gamma_{ion}(R_{div}, s, t) ds \tag{2}$$

where s is the poloidal distance along the target plate and R_{div} is the major radius at the corresponding probe tip. The particle flux of ELMs is given by

$$\Gamma_{ion,ELM} = \left(\frac{\int_{t_{start}}^{t_{end}} \Gamma_{tot}(t) dt}{t_{end} - t_{start}} \right)_{ELMs} - \left(\frac{\int_{t_{start}}^{t_{end}} \Gamma_{tot}(t) dt}{t_{end} - t_{start}} \right)_{inter-ELMs} \tag{3}$$

where t_{start} and t_{end} are the start time and end time of each ELM and inter-ELM in the chosen time interval. The statistic result is shown in figure 6. The linear fitting is applied and the correlation of the fit is quantified by correlation coefficient ($-1 \leqslant CC \leqslant 1$, 1 means positive linear correlation, -1 means negative correlation and 0

means no linear correlation). A positive correlation (CC = 0.55) between ELM size and toroidal rotation is found, consistent with our experimental observation and result in JT-60U [11, 12].

We note that toroidal rotation is not the only factor that affect the ELM size. Other parameters include the collisionality of pedestal plasma, edge magnetic shear, etc. It has been well recorded across worldwide machines that the Type I ELM plasma energy loss normalized to the pedestal energy decrease with increasing collisionality of the pedestal plasma ν^*_{ped} [21]. The data scattering in figure 6 (a) may be due to large variation of plasma parameters in 66 shots, such as auxiliary heating power and plasma density. In fact, the dependence between ELM size and plasma density is found, which shows a negative correlation (CC = *-0.50*) in figure 6 (c). At a given pressure, collisionality is proportional to the cube of the density. The recorded negative correlation between ELM size and plasma density is qualitatively consistent with collisionality scaling of ELM energy losses. The synergistic effect of V_{T0} and n_e on ELM size is shown in figure 7.

Another characteristic is the ELM frequency. In figure 3, ELMs are totally suppressed with sufficient the counter-I_p NBI torque, meanwhile the ELM frequency is decreasing from 100 Hz to 0. This trend is qualitatively consistent with rather weak positive correlation (CC = *0.15*) recorded in figure 6 (b). Two factors should be taken into account. Firstly, the power dependences of ELM frequency in type-I and type-III ELMs are different. Unlike the case in JT-60U [11], there is no perpendicular NBI in EAST to keep absorbed heating power constant when scanning toroidal rotation torque. Secondly, we used a combination of RF heating and NBI heating in the experiment, with large variation in the ratio of NBI power. It was reported that two different dependences of ELM frequency with heating power exist in the "RF dominated heating" ($0.4 < P_{NBI}/P_{NBI+LHW} < 0.55$) and "NBI dominated heating" ($0.67 < P_{NBI}/P_{NBI+LHW} \leqslant 1$) regimes in EAST [22].

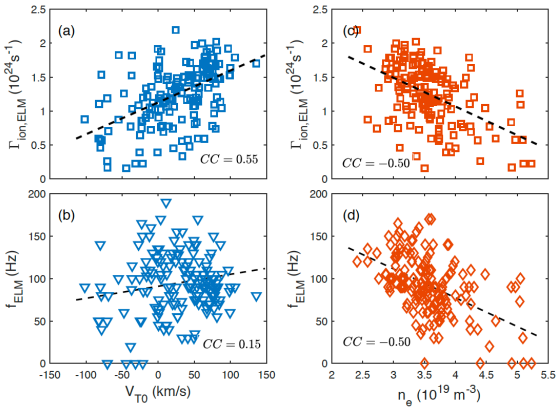

Figure 6. Statistic correlation between (a) ELM-induced ion flux $\Gamma_{ion,ELM}$, (b) ELM frequency f_{ELM} and central toroidal rotation velocity VT0; (c) ELM-induced ion$\Gamma_{ion,ELM}$, (d) ELM frequency f_{ELM} and line-averaged plasma density ne. Correlation coefficient (CC) represents the degree of linear dependence. The dash line is given by linear fitting.

3. POSSIBLE EXPLANATIONS FOR THE ELM MITIGATION/SUPPRESSION REGIME

The onset of type-I ELM instability can be successfully explained by the ideal peeling-ballooning (P-B) theory in the pedestal, where the steep pressure gradient drives ballooning mode and bootstrap current generates peeling mode [23]. Pure ballooning modes can be limiting at high collisionality, and pure kink/peeling modes at low collisionality. EAST is operated under a relatively high collisionality ν^*_{ped} regime. Linear simulation by BOUT++ showed that the dominant peeling-ballooning mode is ballooning mode (n = *30 ~50*) for a typical EAST discharge (I_p = *500 kA*, n_e =*3.5×10^{19}m^{-3}*) [24]. Ideal MHD calculation by ELITE indicates rotation shear can stabilize high-n ballooning modes while destabilizing low-n peeling modes [7]. This may be possible explanation for the ELM suppression regime with sufficient counter-I_p NBI torque (figure 3), as the dominant ballooning mode is stabilized by large rotation shear.

Theory and experiments suggest that large edge $E\times B$ rotational shear is the additional drive mechanism of the EHO in QH-mode [6, 8, 9]. The radial electric field E_r is related to the toroidal rotation from the radial force balance equation:

$$E_r = \frac{\nabla p_Z}{Zen_Z} - v_{\theta,Z} \times B_\psi + v_{\psi,Z} \times B_\theta \qquad (4)$$

where p, Z, n, v denotes the pressure, charge number, density and velocity of the plasma respectively, and r, θ, ψ the radial, poloidal and toroidal direction in the laboratory coordinate. The density profile and Doppler shifted

frequency (f_{DBS} / E_r) profile in shot 56417 is shown in figure 8. The Doppler reflectometry measurement is presented in fDBS instead of Er due to a calibration problem. As it is seen, fDBS or Er forms a typical negative "well" in the pedestal in H-mode, and it becomes larger after transition from co-NBI heating to ctr-NBI heating. Comparison between $t = 3.5s$ and $t = 5.3s$ shows that more toroidal rotation by ctr-NBI may account for the larger E_r, as the density profile (or pressure profile presumably) is similar. Notably, E_r at the end of ctr-NBI phase has decreased to the level of co-NBI phase as the confinement degrades.

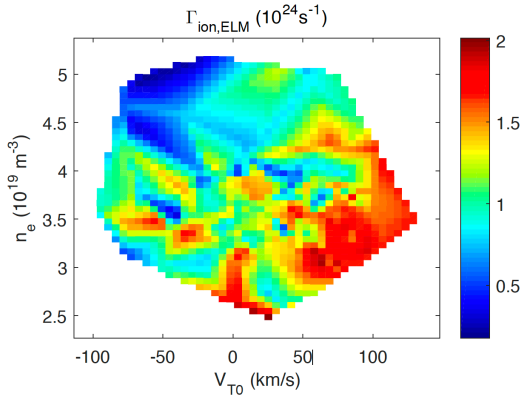

Figure 7. 3-D plot of ELM-induced ion flux $\Gamma_{ion,ELM}$ versus central toroidal rotation velocity V_{T0} and line-averaged plasma density n_e.

A ballooning-like mode with the frequency of *1~2 MHz* was observed in ctr-NBI phase by Doppler reflectometry, which replaces the ELM in co-NBI phase as shown in figure 9. The ballooning-like mode can only be seen with detecting frequency of *60~70GHz*, which manifests its location in pedestal region. The increasing frequency of the mode may be correlated with pedestal density climbing up in ctr-NBI phase. As an alternative to ELMs, this mode is inefficient in producing particle and energy transport to maintain a stationary confinement. Auto-power analysis indicates the turbulence amplitude is higher during ctr-NBI phase than co-NBI phase.

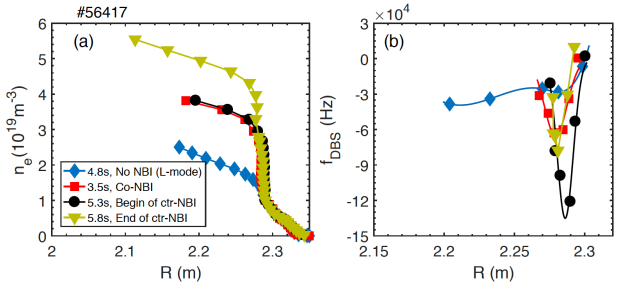

Figure 8. Comparison of (a) density profile and (b) Doppler shifted frequency or radial electric field f_{DBS} / E_r in shot 56417. Four time moments are selected from Co-NBI H-mode, L-mode, the begin and end time of Ctr-NBI H-mode in figure 4.

Nonlinear simulations are needed to understand ELM associated particle and heat losses. Nonlinear BOUT++ simulation by Xu *et al*: [25] has succeed in explaining the impact of pedestal plasma density on ELM crashes, which is consistent with collisionality scaling of ELM energy losses. Another BOUT++ simulation by Kong et al: [26] has investigated the synergistic effect of E_r and collisionality on ELM size: for the high collisionality case, the increased Er shear will suppress the energy transport contributed by ELMs. This trend is consistent with our experimental observation, although the role of rotation shear and E_r shear has yet undistinguished.

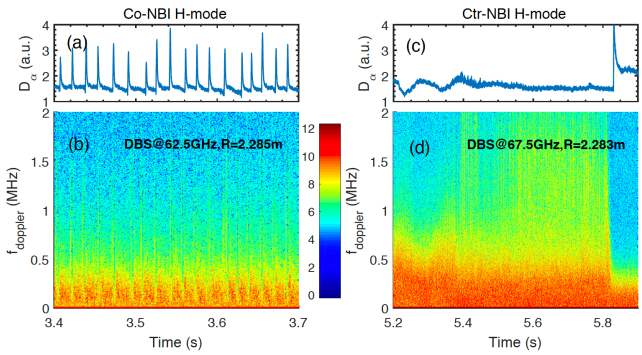

Figure 9. Power spectrum of Doppler reflectometry in shot 56417. (a) D_α signal, (b) density fluctuation of Co-NBI H-mode phase by 62 GHz Reflectometry and (c) D_α signal, (d) density fluctuation of Ctr-NBI H-mode phase by 67.5 GHz Reflectometry. The position of Doppler cut-off surface is shown in figure 8 (b).

Recently, a nonlinear criterion for the occurrence of ELMs is proposed by Xi *et al*: [27]. As it is shown, phase coherence time between potential and pressure perturbations must be long enough to allow growth to large

amplitude, which is determined by both linear drive and nonlinear wave-wave interaction. As it is discussed by Kong *et al*: [26], the enhanced radial electric field in the edge can enhance the nonlinear coupling of underlying modes, and shorten the phase coherence time of the linear growth stage for ELMs.

4. SUMMARY

In this study, we have demonstrated effective ELM mitigation/suppression by ctr-NBI heating in recent EAST experiments. ELMs are strongly mitigated and finally suppressed with increasing toroidal rotation in counter-Ip direction, meanwhile the ELM frequency is decreasing as seen in figure 3 (e-h). In contrast with the stationary H-mode without large ELMs in JT-60U [10, 21], ineffective plasma density control with impurity accumulation and confinement degradation was observed in the ELM suppression regime in EAST. The reason for this difference remains unclear.

A deeper edge Er well was found in ELM mitigation/suppression regimes, because of more toroidal torque input by ctr-NBI heating. Two possible explanations for our experiment result are proposed. First, linear stability analysis indicates edge rotation shear would stabilize high-n ballooning mode [7], which is the dominant P-B mode in high collisionality regime in EAST [24]. Second, nonlinear BOUT++ simulation [26] shows that the nonlinear coupling of underlying modes is enhanced with larger edge Er, which shorten the phase coherent time for ELM growth. However, the exact role of plasma rotation shear and E _ B ow shear are not clarified yet. Further studies are left for the future.

ACKNOWLEDGEMENTS

The authors thank the BOUT++ Team for support of these simulations, Lyu Bo, Guosheng Xu, Zhibin. Guo, Adi Liu, Tianyang Xia, Yong Liu and Mickey Wade for the helpful comments. This work was performed under the auspices of the U.S. DOE by LLNL under Contract No. DE-AC52-7NA27344 and is supported by the Major / Innovative Program of Development Foundation of Hefei Center for Physical Science and Technology No.2018CXFX010, the China National Fusion Project for ITER under No.2014GB106003, and U.S. DOE under Award No. DE-FG02-04ERS4738.

REFERENCES

[1] Perkins F W et al. 1999 Nuclear Fusion 39 2137{2174
[2] Lang P T et al. 2013 Nuclear Fusion 53
[3] Lang P T et al. 2004 Nuclear Fusion 44 665{677
[4] de la Luna E et al. 2016 Nuclear Fusion 56
[5] Becoulet M et al. 2014 Physical Review Letters 113
[6] Burrell K H et al. 2002 Plasma Physics and Controlled Fusion 44 A253{A263
[7] Snyder P B et al. 2007 Nuclear Fusion 47 961{968
[8] Burrell K H et al. 2009 Nuclear Fusion 49
[9] Garofalo A M et al. 2011 Nuclear Fusion 51
[10] Sakamoto Y et al. 2004 Plasma Physics and Controlled Fusion 46 A299{A304
[11] Kamiya K et al. 2006 Plasma Physics and Controlled Fusion 48 A131{A139
[12] Oyama N et al. 2005 Nuclear Fusion 45 871{881
[13] Zuo G et al. 2010 Plasma Science and Technology 12 646{650
[14] Lyu B et al. 2014 Review of Scientific Instruments 85
[15] Zhang L et al. 2015 Review of Scientific Instruments 86
[16] Liu J B et al. 2016 Nuclear Fusion 56
[17] Wang Y M et al. 2013 Fusion Engineering and Design 88 2950{2955
[18] Zhou C et al. 2013 Review of Scientific Instruments 84
[19] Ming T et al. 2009 Fusion Engineering and Design 84 57-63
[20] Wang L et al. 2012 Nuclear Fusion 52
[21] Loarte A et al. 2003 Plasma Physics and Controlled Fusion 45 1549{1569
[22] Zang Q et al. 2016 Nuclear Fusion 56 106003
[23] Snyder P B et al. 2002 Physics of Plasmas 9 2037{2043
[24] Liu Z X et al. 2012 Physics of Plasmas 19
[25] Xu X Q et al. 2014 Physics of Plasmas 21
[26] Kong D et al. 2016

[27] Xi P W et al. 2014 Physical Review Letters 112